Promoting effect of Sn on supported Ni catalyst during steam reforming of glycerol

L. F. Bobadilla,[†]* F. Romero-Sarria, M. A. Centeno and J. A. Odriozola

Departamento de Química Inorgánica e Instituto de Ciencia de Materiales de Sevilla (ICMSE). Centro mixto CSIC - Universidad de Sevilla, 49 Av. Américo Vespucio, 41092 Sevilla (Spain)

† Current address: Instituto de Tecnología Química (ITQ). Centro mixto CSIC-Universidad Politécnica de Valencia, s/n Av. de los naranjos, 46022 Valencia (Spain)

*** Corresponding author:** lbobadilla@itq.upv.es

Abstract:

The promoting effect of Sn on the catalytic performance of supported Ni catalyst in the reaction of glycerol steam reforming was studied. The physico-chemical properties of the prepared samples were investigated by X-ray fluorescence (XRF), BET surface area, *in situ* X-ray diffraction (XRD), laser Raman spectroscopy, X-ray photoelectron spectroscopy (XPS), scanning electron microscopy (SEM) and temperature programmed oxidation (TPO) techniques. The characterization results of the samples after reduction treatment (in the same conditions than the activation before catalytic activity measurements) revealed the formation of Ni-Sn alloy. The Sn-doped catalyst exhibited a high activity and it was demonstrated that the Sn addition increase the catalyst stability and durability by decreasing the coke deposition.

Keywords: *Hydrogen production; Sn addition; Coke deposition*

1. Introduction

During the last decades important efforts are ongoing to reduce fossil fuel dependency and greenhouse gas emissions. Among the different possibilities to find a viable option, the use of hydrogen as an energy carrier is considered to be an interesting alternative for the future and could have a crucial role in reducing atmospheric pollution. Biomass is considered as one of the most attractive renewable source for hydrogen production and numerous studies are being directed toward the development of novel technologies to produce hydrogen from biomass [1-4]. Steam reforming of glycerol is an important approach for hydrogen production from biomass. Glycerol is the main by-product generated in the biodiesel production. Biodiesel is one renewable biofuel obtained by catalytic trans-esterification of triglycerides with methanol [5]. About 10 wt.% of glycerol can be produced during the conversion of vegetable oils into biodiesel. The use of glycerol for hydrogen generation is a very advantageous option since its use would decrease the price of biodiesel making it more competitive [6].

The overall reaction of glycerol steam reforming is given by the following equation:

$$C_3H_8O_3 + 3H_2O \rightarrow 3CO_2 + 7H_2 \quad (1)$$

which can be expressed as a combination of glycerol decomposition (2) and the water-gas shift reaction (3):

$$C_3H_8O_3 \rightarrow 3CO + 4H_2 \quad (2)$$

$$CO + H_2O \leftrightarrow CO_2 + H_2 \quad (3)$$

Theoretically, a maximum of 7 moles of H_2 per mol of glycerol can be produced, although this ratio depends on the reaction conditions such as temperature, pressure and steam-to-glycerol steam ratio.

Although the glycerol steam reforming process is very attractive and it could be developed on an industrial-scale, it has some challenges that must to be overcome in order to accomplish its effective commercialization. For example, the process is an endothermic reaction and requires high temperatures increasing the operation costs. Besides, the catalyst deactivation by coke deposition is also an issue since it affects hydrogen yield and long term operation. With the aim of overcoming these challenges, the development of active, stable and inexpensive catalytic materials is mandatory. Catalysts containing group 8-10 metals such as Ni [7-12], Co [13-16], Pt [17-21], Ru

[22-24], Rh [25], Pd [26] or Ir [27] on different oxides have been largely investigated as active catalysts for glycerol steam reforming. Ni-supported is one of the most promising active metals for such an application because of its high activity, low cost and wide availability. However, Ni-based catalysts suffer deactivation by coke deposition on the catalyst surface that block active sites and favour side reactions. Deactivation of nickel-based catalysts by sintering of nickel crystallites is another important drawback. Promoting nickel catalysts with a second metal has been proven to be one of the most promising approach to obtain more stable and optimal catalysts [28]. Bimetallic catalysts comprising Sn as a Ni promoter have been proved to outperform Ni monometallic catalyst in steam reforming processes [29]. The coke deposition can be markedly reduced by using Sn-doped catalysts in the steam reforming reaction to generate hydrogen from hydrocarbons. Sn alloyed with nickel prevents the formation of nickel atom ensembles, which are the responsible of the coke formation, and avoids the diffusion of carbon to form larger coke agglomerates [30]. Therefore, NiSn-based catalysts have the potential to decrease the catalyst deactivation caused by coking maintaining its high specific activity. Sn-doped Ni catalysts have been reported for aqueous phase reforming [31, 32] and methane steam reforming [33] where the formation Ni_xSn_y alloys play a key role to inhibit coke deposition. Pengpanich et al. [34] reported a clear example of this positive effect in the partial oxidation of iso-octane. These authors found that the addition of small amounts of tin decreased by more than 50% the formation of carbon deposits without changes in the conversion. This enhancement was ascribed to the ability of Sn to reduce the growth of carbon filament by retarding carbon solubility in the Ni particles [28]. Moreover, Saadi et al. [35] have demonstrated, using density functional theory (DFT) calculations, the ability of Ni-Sn to inhibit graphite formation during steam reforming reactions. They demonstrated that the presence of Sn increases the C-C bond formation barrier.

We have investigated previously the effect of the nature of the support (acidity, basicity and redox properties) in the catalytic performance of Sn-doped Ni catalysts during the steam reforming of alcohols [36-38]. The objective of the present work is to investigate the effect of tin on the catalytic performance of Ni-supported catalysts in terms of activity, selectivity and durability in the steam reforming of glycerol.

2. Experimental

2.1. Catalysts preparation

The alumina support was obtained by ball milling spherical alumina pellets (*SASOL*, 1.78 mm diameter), by using a PM4 Retsch instrument particle sizes in 7 – 8 μm range were achieved. A monometallic Ni-based catalyst was prepared by impregnating the alumina with an aqueous solution of all the inorganic precursors with the desired concentrations of cerium (III) nitrate hexahydrate (*Sigma-Aldrich*), magnesium nitrate hexahydrate (*Sigma-Aldrich*), and nickel (II) nitrate hexahydrate (*Sigma-Aldrich*). Then, the sample was dried overnight at 100ºC and calcined at 700ºC for 12 h in flowing air using a heating rate of 10 C min^{-1} to obtain 20 wt.%Ni, 12 wt.%CeO_2, 8 wt.%MgO, and 60 wt.%Al_2O_3. The bimetallic NiSn catalyst was prepared following the same procedure but substituting a fraction of the nickel salt by the adequate amount of anhydrous tin chloride (*Fluka*) in order to obtain 17 wt.%Ni, 3 wt.%Sn, 12 wt.%CeO_2, 8 wt.%MgO, and 60 wt.%Al_2O_3. The resulting catalysts were labelled as Ni/CeMgAl and Ni-Sn/CeMgAl, respectively.

2.2. Materials characterization

The chemical composition of the samples was determined by X-ray fluorescence (XRF) spectroscopy in a Panalytical AXIOS PW4400 sequential spectrometer with Rh tube as source of radiation. The analysis were carried out onto pressed wafers containing 6 wt.% of wax. The textural properties (BET surface, pore size and pore volume) were studied by nitrogen physical adsorption-desorption isotherms at 77 K with Micromeritics ASAP 2010 equipment. Before each measurement, the samples were outgassed for 2 h at 150ºC in vacuum to remove the adsorbed impurities. X-ray diffraction (XRD) analysis was performed on a Siemens D-500 diffractometer using Cu Kα radiation (40 mA, 40 kV) and a position-sensitive detector using a step size of 0.05º and a step time of 1 s. The reducibility of the catalysts was investigated by *in situ* XRD analysis using a high temperature camera Anton Paar HTK 1200 coupled with an X´Pert Pro Philips diffractometer. The system was equipped with X´Celerator detector with a step of 0.05º and an equivalent time acquisition of 30 s. The diffractograms were recorded in the 25 – 900ºC temperature range under a flow of 100 mL min^{-1} (5% H_2 in Ar). Surface characterization was carried out by X-ray photoelectron microscopy (XPS) on a Leybold-Heraeus spectrometer (LHS-10/20), working with a constant pass energy of 50 eV and vacuum of 5 x 10^{-9} Torr. The system was equipped with an EA-200 MCD hemispherical electron analyser with a dual X-ray source working with Al Kα radiation (1486.6 eV) at 120 W and 30 mA. Binding energies were referenced to the spurious C

(1s) signal at 284.6 eV and the atomic composition was estimated by the elemental sensitivity factor of each atom. Before each analysis, the sample was reduced in an external tube furnace for 1 h at 750ºC under a total flow of 100 mL min^{-1} (50% H_2 in N_2). Then, the sample was cooled down to room temperature and placed in the prechamber of the XPS spectrometer. The morphology of the catalysts was evaluated by SEM using a JEOL 5400 instrument equipped with an Energy Dispersive X-ray Spectrometer (OXFORD LINK TETRA 1128-231).

Raman spectra were recorded in a dispersive Horiva Jobin Yvon LabRam HR800 Confocal Raman microscope with a green laser (532.05 nm) working at 5 mV power and using a 600 grooves/mm grating. The microscope used a 50x objective with confocal pinhole of 1000 μm. The Raman spectrometer was calibrated using a silicon wafer. The temperature-programmed oxidation (TPO) was carried out in a U-shaped reactor under a total flow of 50 mL min^{-1} (5% O_2 in He) from room temperature to 900ºC with heating rate of 10 ºC min^{-1}. The formed products were analysed by mass spectrometry (MS) in a Pfeiffer vacuum mass spectrometer.

2.3. Catalytic performance

The glycerol steam reforming reaction was evaluated as a function of time for periods of 4, 12 and 24 h in isothermal conditions at 750ºC, with a steam-to-carbon molar ratio of 4 and 100000 mL g^{-1} h^{-1} space velocity. Prior to reaction, the samples were pressed, crushed, and sieved to achieve particles in the 100-200 μm range. In each run, 100 mg of sample was diluted with the same amount of crushed quartz sieved to the same particle size and placed into the reactor between two quartz wool plugs. The catalysts were activated under a total flow of 100 mL min^{-1} (50% H_2 in N_2) at 750ºC for 1 h. The experiments were carried out at atmospheric pressure in a commercial Microactivity Reference Reactor made by PiD Eng&Tech using a Hastelloy C-276 tubular reactor with 9 mm internal diameter. Gas products were analysed on-line using a microGC (Varian 4900) equipped with Porapak Q and Molecular Sieve – 5A columns. At the reactor outlet a Peltier liquid cooler was fitted allowing the analysis of condensable products by HPLC (Varian 356-LC) equipped with a refractive index detector and a Hi-Plex H column with milli-Q water as eluent.

3. Results and discussion

3.1. Catalysts characterization

Table 1 shows the chemical compositions and textural properties (BET surface, pore size and pore volume) of the prepared catalysts. For comparison, the support was also measured. The experimental compositions of all samples were close to the nominal ones confirming the effectiveness of the impregnation method employed to prepare the catalysts. The parent support presents superior BET surface area, which decreases after Ni or Ni-Sn addition caused by the incorporation of metal particles into the pores of the support.

Figure 1 shows the XRD patterns recorded for the prepared catalysts. The diffraction peaks at 2θ = 28.8º, 33.3º, 47.7º and 56.6º can be assigned to the (111), (200), (220) and (311) planes of the cubic fluorite phase characteristic of cerium oxide (JCPDS 34-0394). It can also be observed the diffraction lines corresponding to the $MgAl_2O_4$ spinel phase (JCPDS 21-1152). As described in a previous work [38] the presence of nickel induces the transformation of the $MgAl_2O_4$ spinel structure into a continuous MgNi spinel layer although only a part of nickel partially substitute Mg in the $MgAl_2O_4$ phase forming a new $Ni_xMg_yAl_2O_4$ phase. Diffraction peaks characteristic of nickel oxide (JCPDS 71-1179) were observed at 37º and 43º. Therefore, it can be established that a fraction of Ni is well dispersed as NiO particles with moderate interaction with the support and another portion of Ni is incorporated within the non-stoichiometric spinel-like phase $Ni_xMg_yAl_2O_4$ [8] with strong metal-support interaction. XRD peaks associated to Sn phases were not observed in the Ni-Sn/CeMgAl catalyst likely due to its high dispersion.

In order to analyse the evolution and the changes in the crystalline phases produced under reductive conditions, *in situ* X-ray diffraction analyses were performed. Reduction was carried out in an atmosphere of hydrogen diluted in Ar. The obtained X-ray diffractograms as a function of temperature are shown in Fig. 2. In both cases, the structural modifications are only appreciable in the high temperature range (700-900 ºC). For the Ni/CeMgAl catalyst, the $Ni_xMg_yAl_2O_4$ and NiO phases are reduced to metallic nickel (JDPDS 45-1027), whereas the reduction of the NiSn/CeMgAl catalyst leads to the formation of Ni_xSn_y alloys coexisting with metallic Ni particles. It is known that nickel can be completely alloyed with tin forming Ni_3Sn, Ni_3Sn_2 and/or Ni_3Sn_4 intermetallic compounds depending of the Ni/Sn molar ratio [39]. In our case, the characteristic peaks of the Ni_3Sn alloy (JCPDS 35-062) were evidenced although the presence of other Ni_xSn_y intermetallic compounds cannot be ruled out. In both cases,

metallic nickel was also present after reduction at 700 ºC. A further increase of the temperature to 900 ºC led to an increase of the Ni diffraction lines, which indicate a sintering of the nickel particles.

Surface analysis measurements by XPS were performed over Ni/CeMgAl and Ni-Sn/CeMgAl catalysts to investigate the chemical surface properties and oxidation states of both metals. Prior to XPS analysis, fresh catalysts were reduced for 1 h at 750ºC under flowing hydrogen diluted in inert to get information about the chemical state of the activated catalysts. Ni 2p and Sn 3d XPS spectra are shown in Fig. 3. Both Ni/CeMgAl and Ni-Sn/CeMgAl catalysts exhibited two deconvoluted $Ni2p_{3/2}$ core-level peaks with the corresponding satellite peaks positioned to ~6 eV, respectively; the peak at 856 eV can be assigned to nickel aluminate phase, while that the peak at 853 eV was attributed to metallic nickel [40, 41]. It was observed that the relative amount of nickel species incorporated in the non-stoichiometric spinel-like phase $Ni_xMg_yAl_2O_4$ is similar in both catalysts while that the relative quantity of metallic nickel is slightly superior in the Ni/CeMgAl catalysts. This observation is coherent with the chemical composition of the catalysts suggesting that the additional nickel in the Ni/CeMgAl catalyst is highly dispersed over the support as nickel oxide crystallites. From the XPS results, it is evident that only the crystalline nickel oxide was reduced and the nickel with strong interaction with the support requires higher temperatures. Both Ni/CeMgAl and Ni-Sn/CeMgAl catalysts exhibited identical amount of nickel aluminate species strongly bound to the support which were not reduced under our conditions at 750ºC. The reduction of Ni^{2+} ions incorporated non-stoichiometrically in tetrahedral or octahedral sites of spinel phases requires temperatures as high as 800-850 ºC [42].

The Sn 3d region spectra for the Ni-Sn/CeMgAl catalyst is shown in Fig. 3. The peak at 485 eV can be assigned to Sn^0 species while that the higher binding energy $Sn\ 3d_{5/2}$ peak at 487 eV is attributable to tin oxides (Sn^{2+} or Sn^{4+}) [32]. The reduced species of tin is probably a Ni-Sn alloy. Discriminating between Sn^{2+} and Sn^{4+} with XPS is complicated, but the presence of this species indicates that the reduction of tin was not complete, and oxidized species are existent even after reduction at 750 ºC, in agreement with previous results on alumina-supported catalysts [43]. Alumina interacts strongly with the tin and hinders the redution of SnO [44]. Thererefore, XPS analysis of the Ni-Sn/CeMgAl after reduction at 750ºC indicates the presence of Ni and Sn separate phases. The ongoing reduction of Ni and Sn can be concurrent with the formation of a

Ni-Sn alloy, however this alloys are indistinguishable by XPS from reduced Ni surfaces [32]. Consequently, it can be proposed that the Ni-Sn catalyst after activation may be represented by the formation of bimetallic particles with a central core of nickel surrounded by an outer layer rich in tin (Fig. 3). During the reduction phase, a part of Sn atoms migrate to the metallic nickel particles surface to form a Sn layer that is partially reduced forming a Ni-Sn alloy covering the surface of Ni particles. As can be observed in Table 2, the surface Ni/Sn determined by XPS was lower than the bulk one suggesting that Sn is located mainly in the surface layers of the catalyst. Similar observations were found by other authors in the literature [34, 45].

3.2. Activity measurements

The catalyst performances were tested for the hydrogen production in the glycerol steam reforming. Figure 4 shows the specific activity for both Ni/CeMgAl and Ni-Sn/CeMgAl catalysts. It is noteworthy that the catalytic behaviour was different in both cases. The activity for Ni/CeMgAl catalyst was found to be higher than that of the Sn-promoted one and, apparently, very stable for the first 12 hours. Once this period is reached the catalytic activity drastically decreases suggesting a fast deactivation process. The partial substitution of Ni by Sn in the NiSn/CeMgAl catalyst reduces the catalytic activity but notably enhances the stability of the catalyst. As can be observed, after an initial stabilization period for the first 4 hours, the catalytic activity remains stable. The observed activity loss upon tin addition might be due to the fact that the nickel active sites for the glycerol steam reforming are covered by Sn species as confirmed by XPS analysis. The Sn-enriched surface prevents the adsorption of the glycerol molecules on the metallic nickel surface and the subsequent reforming reactions. Similar observations were early reported in the literature for the NiSn/$Ce_{0.75}Zr_{0.25}O_2$ [34] and PtSn/C [46] systems.

The same gaseous products were detected in both catalysts (H_2, CO, CO_2, CH_4 and C_2H_4, Figure 5), although with a different product distribution. Condensable products such as oxygenated compounds were not detected at this reaction temperature in good agreement with previous results [36]. Hydrogen was the main component in both catalysts and remained invariant during all time-on-stream. It can be noticed that during the first 12 hours, the Ni/CeMgAl catalyst produced the maximum hydrogen molar fraction possible (70%) according to the stoichiometry of the reaction (1). After 12 h of reaction changes in the molar composition were observed. From here, the production of

CO_2 decreases along with the increase of CO, CH_4 and C_2H_4. Moreover, the change of selectivity appears when activity loss is observed. For the Ni-Sn/CeMgAl catalyst, an increase of CO and decrease of CO_2 started from the beginning of the reaction while that CH_4 and C_2H_4 were produced continuously.

The differences observed in both cases would be associated to the catalytic processes involved in the glycerol decomposition process. The overall reaction of glycerol steam reforming (1) may be viewed as the combination of the glycerol decomposition (2) and the water gas shift (WGS) reaction (3). Furthermore, it may also be accompanied by other thermodynamically feasible reactions that include:

$$2C_3H_8O_3\,(g) + H_2\,(g) \leftrightarrow 3CH_4\,(g) + 3CO\,(g) + 3H_2O\,(g) \quad (4)$$

$$CO\,(g) + 3H_2\,(g) \leftrightarrow CH_4\,(g) + H_2O\,(g) \quad (5)$$

$$CO_2\,(g) + 4H_2\,(g) \leftrightarrow CH_4\,(g) + 2H_2O\,(g) \quad (6)$$

$$CO_2\,(g) + CH_4\,(g) \leftrightarrow 2CO\,(g) + 2H_2\,(g) \quad (7)$$

$$C(s) + H_2O\,(g) \rightarrow CO\,(g) + H_2\,(g) \quad (8)$$

$$C(s) + CO_2\,(g) \leftrightarrow 2CO\,(g) \quad (9)$$

$$C(s) + 2H_2\,(g) \leftrightarrow CH_4\,(g) \quad (10)$$

The initial gas products distribution for Ni/CeMgAl catalyst indicates that the WGS reaction was predominant in the first 12 h. This is consistent with a production of hydrogen close to the equilibrium value. After 12 h of reaction methane and ethylene are produced. Araque et al. [13] suggested that the formation of methane proceeds through carbon monoxide methanation (5) while ethylene would be originated by hydrogenation/dehydration of carbonyl intermediates species. Cheng et al. [47] proposed, however, that methane is produced from the hydrogenolysis of glycerol (4) ruling out the methanation reaction as path for methane production. The stable production of methane for Ni-Sn/CeMgAl catalyst suggests that methane could be originated predominantly from the glycerol hydrogenation and the carbon hydrogenation (10). Indeed, the steam gasification of carbon (8) and the Boudouard reaction (9) may also account for the increased stability of Ni-Sn catalyst reducing the deposition of carbonaceous species while the production of CO and H_2 keeps constant. CO formation on Sn is the favoured reaction from CO_2 decomposition, especially for

NiSn (110) and NiSn (111) planes, and the O concentration at surface from CO_2 dissociation when Sn is present, could be high enough to avoid the C formation [33]. Therefore, the observed trends may be understood considering the oxidation rate of the carbonaceous deposits. The influence of tin on the oxidation of carbonaceous species is reflected in the product distribution.

It is well known that carbon species in nickel step sites are stable and its reaction/gasification is difficult. If these adsorbed carbon species disappear at low rate, the carbonaceous species are accumulated on the metallic surface and its concentration is high enough to initiate the diffusion in the metallic particle and the growth of carbon nanotubes. Then, the evolution of the catalytic performance as a function on time on stream must be associated to the coke formation. Nikolla et al. [29] demonstrated using DFT calculations that the presence of Sn increases the barrier for C-C bond formation. According to these authors, the presence of tin preferentially oxidize C atoms rather than form C–C bonds and decreases the carbon nucleation on the low-coordinated sites. Our results of activity and selectivity suggest a modification of the electronic structure of Ni in the presence of Sn which led to the creation of new sites able to modify the adsorption capacity of hydrocarbons by electronic and geometrical effects.

3.3. Study of carbonaceous deposits

Considering that the tin addition to the catalyst was performed in order to enhance the coking resistance, we have evaluated the formation of carbonaceous species by different characterization techniques such as SEM, Raman spectroscopy, temperature-programmed oxidation (TPO), and XPS analysis of the spent catalysts after different times of reaction in order to gain information about the quantity and nature of the coke formed on the solid.

SEM micrographs of the fresh and spent catalysts are shown in Fig. 6. It can be observed that both fresh catalysts presented a similar morphology. After 4 h of reaction, the Ni/CeMgAl catalyst exhibits a high concentration of coke deposits in which, carbon filamentous and nanofibers are noticed. For the Ni-Sn/CeMgAl catalyst some rod-like carbon can be observed highly dispersed over the surface. After 24 h of reaction, the surface of Ni/CeMgAl catalyst appears completely coated by carbon fibers and carbon nanotubes indicating that all the particles area are surrounded by carbon. The growth in length of filamentous coke is observed in all directions and, at the same time, the

support is no longer visible. It might be possible that the decomposition of glycerol and the subsequent formation of carbonaceous species is initiated on Ni active sites and that the formation and growth of filamentous coke causes the rearrangement of the nickel particles on the support surface. This observation is consistent with the opinion of other authors that suggested Ni particle size leads to change in the mechanism of coke formation [48, 49]. As seen from SEM image of Ni-Sn/CeMgAl catalyst, after 24 h of reaction the solid surface is partially coated by filamentous and carbon whiskers, although it seems that the deposits do not cover completely the particle and some active sites remain accessible. It is clearly seen from SEM images that the amount of carbon accumulated decreased after tin addition.

Raman spectroscopy is a useful technique for characterizing the structure of carbonaceous deposits with different degrees of graphitic ordering. Fig. 7 shows the Raman spectra of both fresh and used catalysts after 4, 12 and 24 h of reaction. For both fresh samples a band centered at about 455 cm^{-1} can be ascribed to the F_{2g} Raman mode of ceria fluorite cell corresponding to oxygen symmetric breathing vibration around Ce^{4+} [50]. For Ni/CeMgAl catalyst, two new bands at 1345 and 1583 cm^{-1} can be noticed after 4 h of reaction. These bands were more intense after 12 of reaction and are typical of sp^2-bonded carbon species, which have two main vibrational modes: the G peak around 1580-1600 cm^{-1} and the D peak around 1350 cm^{-1}, usually assigned to phonons of E_{2g} and A_{1g} symmetry, respectively [51]. Conversely for NiSn/CeMgAl, the bands at 1345 and 1583 cm^{-1} only were observed after 24 of reaction. These results demonstrate that the addition of tin favors the catalytic stability and tin seems inhibit the formation of carbonaceous deposits during the glycerol steam reforming in good agreement with the SEM images. It is noteworthy that both D and G bands are very broad, which indicates that coke is presented in different forms (nanocrystalline graphite, carbon nanotubes, amorphous carbon, …). In order to estimate the degree of organization of the carbonaceous deposits, Beyssac et al.[52] proposed the use of the D/(G+D) band area ratio. They suggested that values higher than 0.5 corresponds to poorly organized carbonaceous materials while those lower than 0.5 indicates well organized ones. In our case, the estimated values for Ni/CeMgAl and NiSn/CeMgAl solids after 24 h of reaction were 0.65 and 0.64, respectively. This indicates that carbonaceous species presented a low degree of crystallinity independently of the

amount of carbon deposited or the presence of Sn, in good agreement with the study of catalyst deactivation during methane decomposition on Ni-based catalysts reported by Suelves et al. [53] They found that no difference in the structure of the deposited carbon can be evidenced among active and inactive catalysts.

TPO experiments of the spent catalysts after reaction for 24 h were performed to investigate the nature of the carbonaceous species deposited on the surface of the catalysts. The evolution of CO_2 signal (m/z = 44) was analysed by MS and the results are shown in Fig. 8. Both catalysts presented an intense peak at 730 ºC that indicates the existence of highly structured carbon deposits after 24 of reaction. Considering that the area under the TPO curve is proportional to the amount of deposited carbon it must be stated that the Ni/CeMgAl catalyst produces more quantity of carbon deposits than Ni-Sn/CeMgAl catalyst, which is in accordance with the observed stability for this catalyst. The temperatures at which the maximum of CO_2 production is observed informs about the type of carbonaceous species deposited on the catalyst surface. According to literature [54], the combustion of structured carbon whiskers gives a TPO peak at temperatures higher than 600 ºC. This result indicates the presence of carbon nanotubes in the used catalysts, as previously established from the SEM and Raman analyses. Vicente et al. [55] performed a study about the coke deactivation of Ni and Co catalysts in ethanol steam reforming reaction. They observed that the coke deposited is constituted by two fractions of different nature of which polymeric or encapsulating coke (with TPO peak below 450 ºC) is the main responsible for deactivation by blocking metallic sites. The other fraction of coke is constituted by filamentous carbon (with TPO peaks above 500ºC) that coats catalyst particles and increases their size with time-on-stream with a low effect on deactivation. The absence of peaks below 450ºC in our study suggests that the nature of coke deposited in the Ni- and NiSn-based catalysts is constituted mainly by filamentous carbon and the catalysts should be easily regenerated after the coke combustion with air. In a previous study about the performance of NiSn catalyst, we have demonstrated that the catalyst performance is reproducible in si successive reaction-regeneration cycles [36].

For further identification of chemical status of carbon species formed during glycerol steam refoming both spent catalysts were analysed by XPS. From a quantitative point of view, Table 2 shows the percentage of carbon deposited in both samples. It can be noticed a diminution of the amount of carbonaceous species deposited on adding tin to

the nickel catalyst in good agreement with TPO results. Furthermore, it should be noted that surface nickel sites able to initiate the C-H bond activation remain accesible for NiSn/CeMgAl catalyst after 24 h of reaction. For this reason the Ni-Sn/CeMgAl catalyst presented an optimal catalytic performance after 24 of reaction. The C 1s XPS spectra (Fig. 9) of the used catalysts presented two peaks at 282 and 284.6 eV assigned to coating and filamentous carbon deposited on the catalysts surface [34]. It is noteworthy that the peak area ratio of C 1s decreased for Sn-doped catalyst revealing that the growth of carbon nanotubes is retarded by addition of Sn in accordance with our previous considerations.

From the results and discussion, the beneficial effect of the tin addition to the nickel catalyst is clear for glycerol steam reforming. The incorporation of nickel by the tin promoter modifies positively the performance of the catalyst promoting the gasification of the carbon generated. Moreover, Sn is able to modify the performance of Ni-based catalyst, inhibiting reactions of coke production and thereby improving the catalyst stability. Thus, the deactivation of the catalyst decreases and the process of glycerol steam reforming can operate for longer time.

4. Conclusions

In the present study, it was proven that the presence of Sn on the surface of nickel particles can effectively decrease the growth of carbon nanotubes. Results of characterization (*in situ* XRD and XPS) suggested a core of Ni surrounded by an outer Sn-rich layer. The formation of a surface Ni-Sn alloy generated new sites and modified the adsorption capacity of glycerol. Bimetallic Ni-Sn catalyst showed an optimal performance in terms of activity and stability in the glycerol steam reforming reaction. Results of characterization post-reaction (SEM, Raman, TPO and XPS) demonstrated that tin inhibits the formation of carbonaceous deposits favoring the gasification of coke.

Acknowledgements

Financial support for this work has been obtained from the Spanish MINECO (ENE2009-14522-C05-01) co-funded by FEDER fund from the European Union. Luis F. Bobadilla thanks the Junta de Andalucía for the fellowship granted associated to the project POG-TEP01965.

References

[1] Kalinci Y, Hepbasli A, Dincer I. Biomass-based hydrogen production: A review and analysis. Int. J. of Hydrogen Energy. 2009;34:8799-817.

[2] Parthasarathy P, Narayanan KS. Hydrogen production from steam gasification of biomass: Influence of process parameters on hydrogen yield – A review. Renew. Energy. 2014;66:570-9.

[3] Saxena RC, Seal D, Kumar S, Goyal HB. Thermo-chemical routes for hydrogen rich gas from biomass: A review. Renew. Sustainable Energy Rev. 2008;12:1909-27.

[4] Tanksale A, Beltramini JN, Lu GM. A review of catalytic hydrogen production processes from biomass. Renew. Sustainable Energy Rev.. 2010;14:166-82.

[5] Tasnadi-Asztalos Z, Agachi P-S, Cormos C-C. Evaluation of energy efficient low carbon hydrogen production concepts based on glycerol residues from biodiesel production. Int. J. Hydrogen Energy. 2015;40:7017-27.

[6] Silva JM, Soria MA, Madeira LM. Challenges and strategies for optimization of glycerol steam reforming process. Renew. Sustainable Energy Rev. 2015;42:1187-213.

[7] Cheng CK, Foo SY, Adesina AA. Steam reforming of glycerol over Ni/Al2O3 catalyst. Catal. Today. 2011;178:25-33.

[8] Dieuzeide ML, Jobbagy M, Amadeo N. Glycerol steam reforming over Ni/mg/γ-Al_2O_3 catalysts effect of Ni(II) content. Int. J. Hydrogen Energy. 2014;39:16976-82.

[9] Huang Z-Y, Xu C-H, Meng J, Zheng C-F, Xiao H-W, Chen J, et al. Glycerol steam reforming to syngas over Ni-based catalysts on commercial Linde-type 5A zeolite modified by metal oxides. J. Environ. Chem. Eng. 2014;2:598-604.

[10] Nichele V, Signoretto M, Menegazzo F, Gallo A, Dal Santo V, Cruciani G, et al. Glycerol steam reforming for hydrogen production: Design of Ni supported catalysts. Appl. Catal. B Environ. 2012;111–112:225-32.

[11] Shao S, Shi A-W, Liu C-L, Yang R-Z, Dong W-S. Hydrogen production from steam reforming of glycerol over Ni/CeZrO catalysts. Fuel Process. Technol. 2014;125:1-7.

[12] Rossetti I, Gallo A, Dal Santo V, Bianchi CL, Nichele V, Signoretto M, et al. Nickel Catalysts Supported Over TiO_2, SiO_2 and ZrO_2 for the Steam Reforming of Glycerol. ChemCatChem. 2013;5:294-306.

[13] Araque M, Martínez T LM, Vargas JC, Roger AC. Hydrogen production by glycerol steam reforming over CeZrCo fluorite type oxides. Catal. Today. 2011;176:352-6.

[14] Cheng CK, Foo SY, Adesina AA. H_2-rich synthesis gas production over Co/Al_2O_3 catalyst via glycerol steam reforming. Catal. Commun. 2010;12:292-8.

[15] Brum Pereira E, Ramirez de la Piscina P, Homs N. Efficient hydrogen production from ethanol and glycerol by vapour-phase reforming processes with new cobalt-based catalysts. Biores. Technol. 2011;102:3419-23.

[16] Surendar M, Sagar TV, Babu BH, Lingaiah N, Rao KSR, Prasad PSS. Glycerol steam reforming over La-Ce-Co mixed oxide-derived cobalt catalysts. RSC Adv. 2015;5:45184-93.

[17] de Rezende SM, Franchini CA, Dieuzeide ML, Duarte de Farias AM, Amadeo N, Fraga MA. Glycerol steam reforming over layered double hydroxide-supported Pt catalysts. Chem. Eng. J. 2015;272:108-18.

[18] Pompeo F, Santori GF, Nichio NN. Hydrogen production by glycerol steam reforming with Pt/SiO_2 and Ni/SiO_2 catalysts. Catalysis Today. 2011;172:183-8.

[19] Carvalho DC, Souza HSA, Filho JM, Assaf EM, Thyssen VV, Campos A, et al. Nanosized Pt-containing Al_2O_3 as an efficient catalyst to avoid coking and sintering in steam reforming of glycerol. RSC Adv. 2014;4:61771-80.

[20] Zhang X-H, Yan F-W, Guo C-Y, Yuan G-Q. Steam reforming of glycerol over Pt-MCM-41 synthesized in a one-step process. Russ. J. Phys. Chem. A. 2012;86:1957-61.

[21] Montini T, Singh R, Das P, Lorenzut B, Bertero N, Riello P, et al. Renewable H-2 from Glycerol Steam Reforming: Effect of La_2O_3 and CeO_2 Addition to Pt/Al_2O_3 catalysts. ChemSusChem. 2010;3:619-28.

[22] Kim J, Lee D. Glycerol steam reforming on supported Ru-based catalysts for hydrogen production for fuel cells. Int. J. Hydrogen Energy. 2013;38:11853-62.

[23] Gallo A, Pirovano C, Ferrini P, Marelli M, Psaro R, Santangelo S, et al. Influence of reaction parameters on the activity of ruthenium based catalysts for glycerol steam reforming. Appl. Catal. B Environ. 2012;121:40-9.

[24] Sundari R, Vaidya PD. Reaction Kinetics of Glycerol Steam Reforming Using a Ru/Al_2O_3 Catalyst. Energy & Fuels. 2012;26:4195-204.

[25] Chiodo V, Freni S, Galvagno A, Mondello N, Frusteri F. Catalytic features of Rh and Ni supported catalysts in the steam reforming of glycerol to produce hydrogen. Appl. Catal. A Gen. 2010;381:1-7.

[26] Ebshish A, Yaakob Z, Taufiq-Yap YH, Bshish A, Shaibani A. Catalytic Steam Reforming of Glycerol Over Cerium and Palladium-Based Catalysts for Hydrogen Production. J. Fuel Cell Sci. Technol. 2013;10.

[27] Huang X, Dang C, Yu H, Wang H, Peng F. Morphology Effect of Ir/$La_2O_2CO_3$ Nanorods with Selectively Exposed {110} Facets in Catalytic Steam Reforming of Glycerol. ACS Catal. 2015;5:1155-63.

[28] Dal Santo V, Gallo A, Naldoni A, Guidotti M, Psaro R. Bimetallic heterogeneous catalysts for hydrogen production. Catal. Today. 2012;197:190-205.

[29] Nikolla E, Schwank J, Linic S. Promotion of the long-term stability of reforming Ni catalysts by surface alloying. J. Catal. 2007;250:85-93.

[30] Kan H, Hyun SH, Shul Y-G, Lee H. Improved solid oxide fuel cell anodes for the direct utilization of methane using Sn-doped Ni/YSZ catalysts. Catal. Commun.. 2009;11:180-3.

[31] Shabaker JW, Huber GW, Dumesic JA. Aqueous-phase reforming of oxygenated hydrocarbons over Sn-modified Ni catalysts. J. Catal. 2004;222:180-91.

[32] Shabaker JW, Simonetti DA, Cortright RD, Dumesic JA. Sn-modified Ni catalysts for aqueous-phase reforming: Characterization and deactivation studies. J. Catal. 2005;231:67-76.

[33] Ferreira MaL, Nichio NN, Ferretti OA. A semiempirical theoretical study of Ni/α-Al_2O_3 and NiSn/α-Al_2O_3 catalysts for CH_4 reforming. J. Mol. Catal. A Chem. 2003;202:197-213.

[34] Pengpanich S, Meeyoo V, Rirksomboon T, Schwank J. iso-Octane partial oxidation over Ni-Sn/$Ce_{0.75}Zr_{0.25}O_2$ catalysts. Catal. Today. 2008;136:214-21.

[35] Saadi S, Hinnemann B, Helveg S, Appel CC, Abild-Pedersen F, Nørskov JK. First-principles investigations of the Ni_3Sn alloy at steam reforming conditions. Surf. Sci. 2009;603:762-70.

[36] Bobadilla LF, Penkova A, Álvarez A, Domínguez MI, Romero-Sarria F, Centeno MA, et al. Glycerol steam reforming on bimetallic NiSn/CeO_2–MgO–Al_2O_3 catalysts: Influence of the support, reaction parameters and deactivation/regeneration processes. Appl. Catal. A Gen. 2015;492:38-47.

[37] Bobadilla LF, Penkova A, Romero-Sarria F, Centeno MA, Odriozola JA. Influence of the acid–base properties over NiSn/MgO–Al_2O_3 catalysts in the hydrogen production from glycerol steam reforming. Int. J. Hydrogen Energy. 2014;39:5704-12.

[38] Penkova A, Bobadilla L, Ivanova S, Domínguez MI, Romero-Sarria F, Roger AC, et al. Hydrogen production by methanol steam reforming on NiSn/MgO–Al2O3 catalysts: The role of MgO addition. Appl. Catal. A Gen. 2011;392:184-91.

[39] Onda A, Komatsu T, Yashima T. Preparation and Catalytic Properties of Single-Phase Ni–Sn Intermetallic Compound Particles by CVD of $Sn(CH_3)_4$ onto Ni/Silica. J. Catal. 2001;201:13-21.

[40] Kharat AN, Pendleton P, Badalyan A, Abedini M, Amini MM. Decomposition of Nickel Formate on Sol–Gel Alumina and Characterization of Product by X-Ray Photoelectron and TOF-SIMS Spectroscopies. J. Catal. 2002;205:7-15.

[41] Requies J, Barrio VL, Cambra JF, Güemez MB, Arias PL, La Parola V, et al. Effect of redox additives over Ni/Al_2O_3 catalysts on syngas production via methane catalytic partial oxidation. Fuel. 2008;87:3223-31.

[42] Patcas F, Hönicke D. Effect of alkali doping on catalytic properties of alumina-supported nickel oxide in the selective oxidehydrogenation of cyclohexane. Catal. Commun. 2005;6:23-7.

[43] Bacaud R, Bussière P, Figueras F. Mössbauer spectra investigation of the role of tin in platinum-tin reforming catalysts. J. Catal. 1981;69:399-409.

[44] Serrano-Ruiz JC, Huber GW, Sánchez-Castillo MA, Dumesic JA, Rodríguez-Reinoso F, Sepúlveda-Escribano A. Effect of Sn addition to Pt/CeO_2–Al_2O_3 and Pt/Al_2O_3 catalysts: An XPS, ^{119}Sn Mössbauer and microcalorimetry study. J. Catal. 2006;241:378-88.

[45] Nichio NN, Casella ML, Santori GF, Ponzi EN, Ferretti OA. Stability promotion of Ni/α-Al_2O_3 catalysts by tin added via surface organometallic chemistry on metals: Application in methane reforming processes. Catal. Today. 2000;62:231-40.

[46] Pastor-Pérez L, Merlo A, Buitrago-Sierra R, Casella M, Sepúlveda-Escribano A. Bimetallic PtSn/C catalysts obtained via SOMC/M for glycerol steam reforming. J. Colloid Interf. Sci. 2015;459:160-6.

[47] Cheng CK, Foo SY, Adesina AA. Glycerol Steam Reforming over Bimetallic Co−Ni/Al_2O_3. Ind. Eng. Chem. Res. 2010;49:10804-17.

[48] Vicente J, Ereña J, Montero C, Azkoiti MJ, Bilbao J, Gayubo AG. Reaction pathway for ethanol steam reforming on a Ni/SiO_2 catalyst including coke formation. Int. J. Hydrogen Energy. 2014;39:18820-34.

[49] Montero C, Ochoa A, Castaño P, Bilbao J, Gayubo AG. Monitoring Ni^0 and coke evolution during the deactivation of a $Ni/La_2O_3–\alpha Al_2O^3$ catalyst in ethanol steam reforming in a fluidized bed. J. Catal. 2015;331:181-92.

[50] Reina TR, Ivanova S, Centeno MA, Odriozola JA. Boosting the activity of a $Au/CeO_2/Al_2O_3$ catalyst for the WGS reaction. Catal. Today. 2015;253:149-54.

[51] Dresselhaus MS, Dresselhaus G, Jorio A, Souza Filho AG, Saito R. Raman spectroscopy on isolated single wall carbon nanotubes. Carbon. 2002;40:2043-61.

[52] Beyssac O, Goffé B, Petitet J-P, Froigneux E, Moreau M, Rouzaud J-N. On the characterization of disordered and heterogeneous carbonaceous materials by Raman spectroscopy. Spectrochim. Acta A. 2003;59:2267-76.

[53] Suelves I, Lázaro MJ, Moliner R, Corbella BM, Palacios JM. Hydrogen production by thermo catalytic decomposition of methane on Ni-based catalysts: influence of operating conditions on catalyst deactivation and carbon characteristics. Int J. Hydrogen Energy. 2005;30:1555-67.

[54] Tomishige K, Chen Y-g, Fujimoto K. Studies on Carbon Deposition in CO_2 Reforming of CH_4 over Nickel–Magnesia Solid Solution Catalysts. J. Catal. 1999;181:91-103.

[55] Vicente J, Montero C, Ereña J, Azkoiti MJ, Bilbao J, Gayubo AG. Coke deactivation of Ni and Co catalysts in ethanol steam reforming at mild temperatures in a fluidized bed reactor. Int. J. Hydrogen Energy. 2014;39:12586-96.

TABLES AND FIGURES

Table 1. Chemical composition and textural properties of the prepared catalysts

	wt.% composition[a]					at.% composition			S_{BET}
	Al_2O_3	MgO	CeO_2	Ni	Sn	Ni	Sn	Ni/Sn	($m^2 g^{-1}$)
CeMgAl	77.9 (78)	9.6 (10)	12.5 (12)	-	-	-	-	-	106
Ni/CeMgAl	63.6 (60)	6.6 (7)	11.1 (12)	18.7 (20)	-	27.5	-	-	89
Ni-Sn/CeMgAl	60.1 (60)	6.8 (7)	11.9 (12)	17.3 (17)	3.7 (3)	25.6	2.7	9.4	86

[a] Nominal values in parenthesis

Table 2. Surface composition obtained by XPS analysis of the reduced and spent catalysts

	at.% composition[a]							
	Al	Mg	Ce	O	Ni	Sn	C	Ni/Sn
Ni/CeMgAl reduced	18.7	5.1	2.0	69.5	4.6 (27.5)	-	-	
Ni/CeMgAl spent	-	-	0.15	4.35	-	-	95.5	
Ni-Sn/CeMgAl reduced	17.8	6.1	2.0	69.2	3.7 (25.6)	1.1 (2.7)	-	3.4 (9.4)
Ni-Sn/CeMgAl spent	3.5	2.1	0.4	21.7	0.5	0.1	71.8	5.0

[a] Bulk values in parenthesis

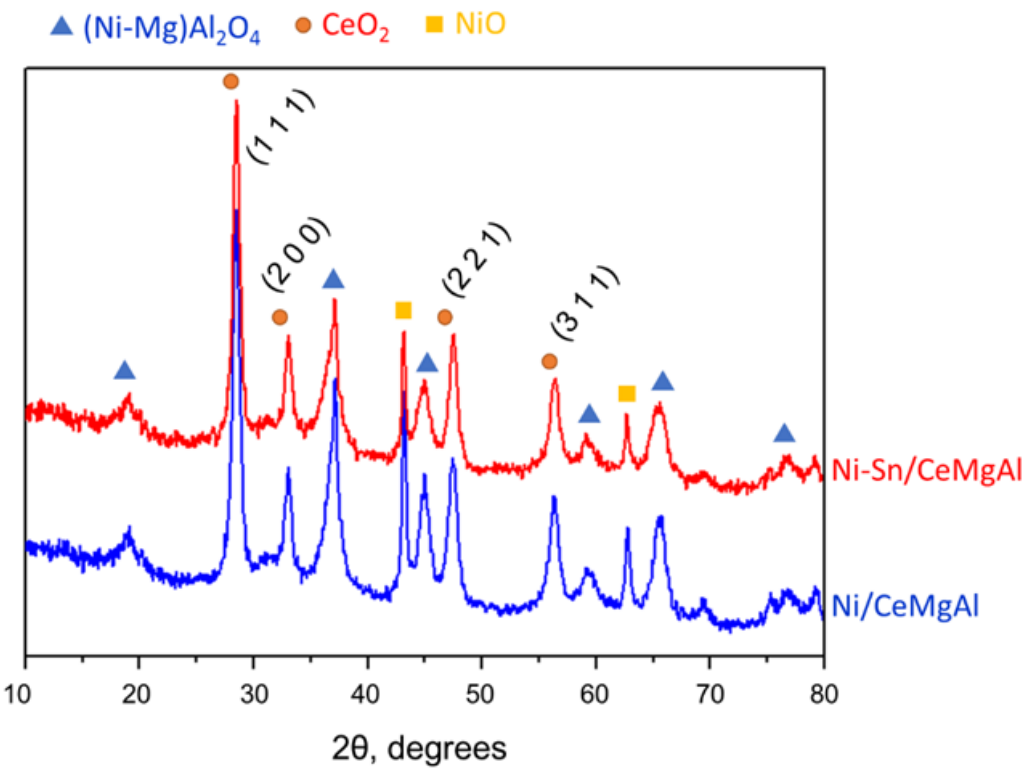

Fig. 1 XRD patterns for the prepared catalysts

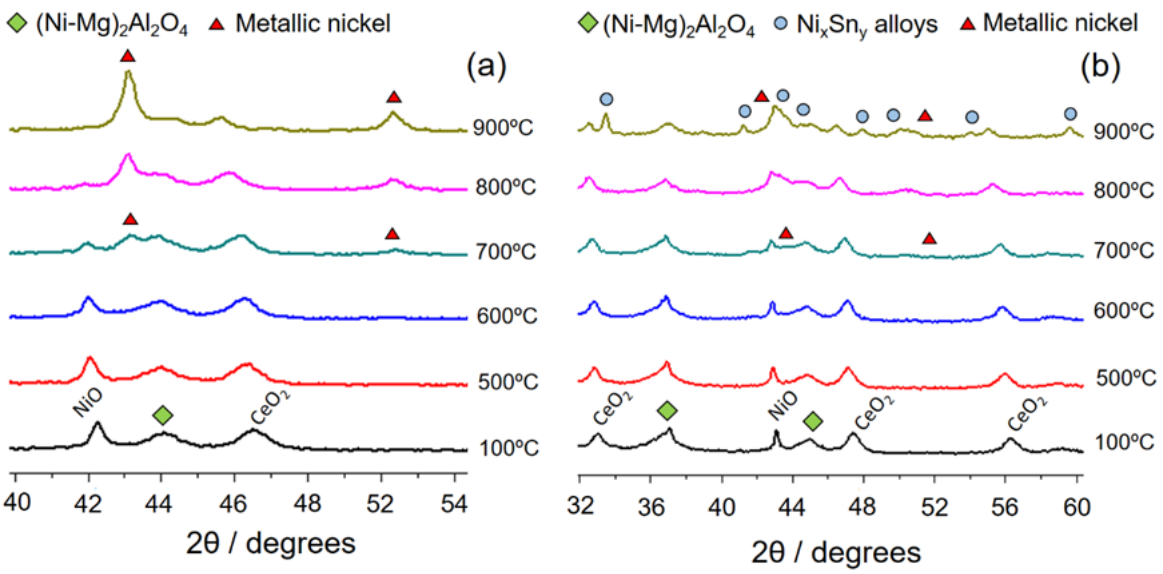

Fig. 2 *In situ* XRD patterns in reductive atmosphere for the prepared catalysts: (a) Ni/CeMgAl and (b) Ni-Sn/CeMgAl

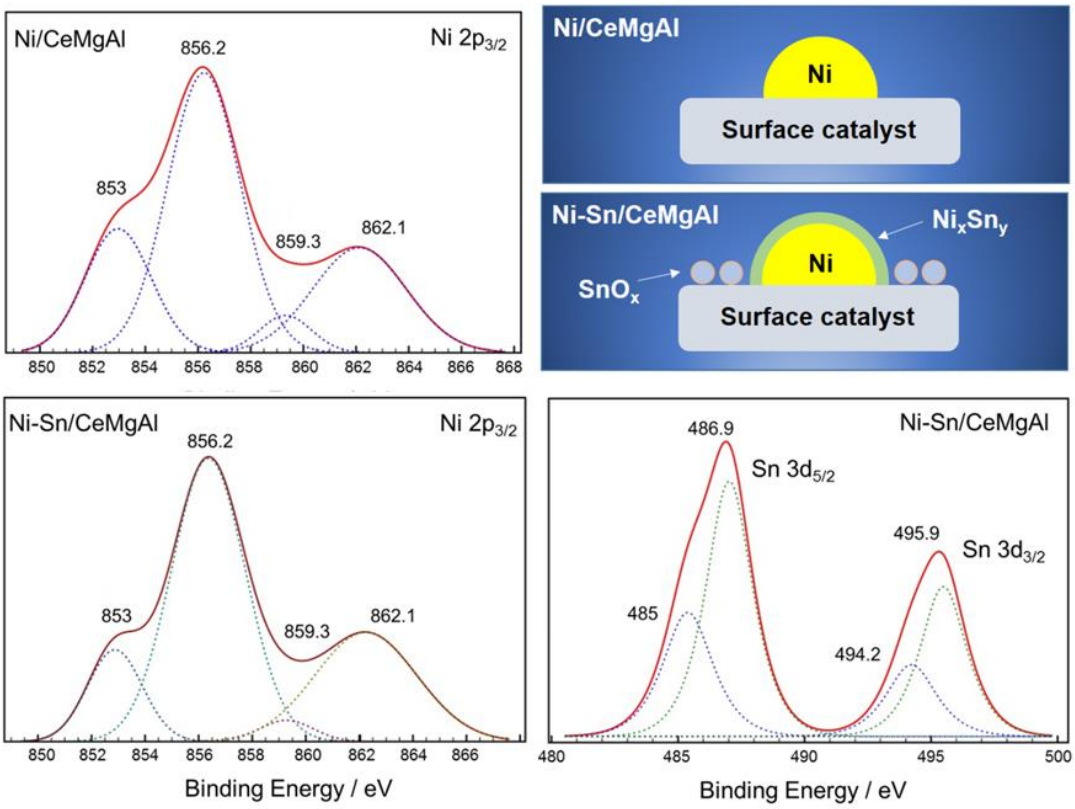

Fig. 3 XPS spectra in the Ni 2p and Sn 3d level and pictorial representation of reduced catalyst

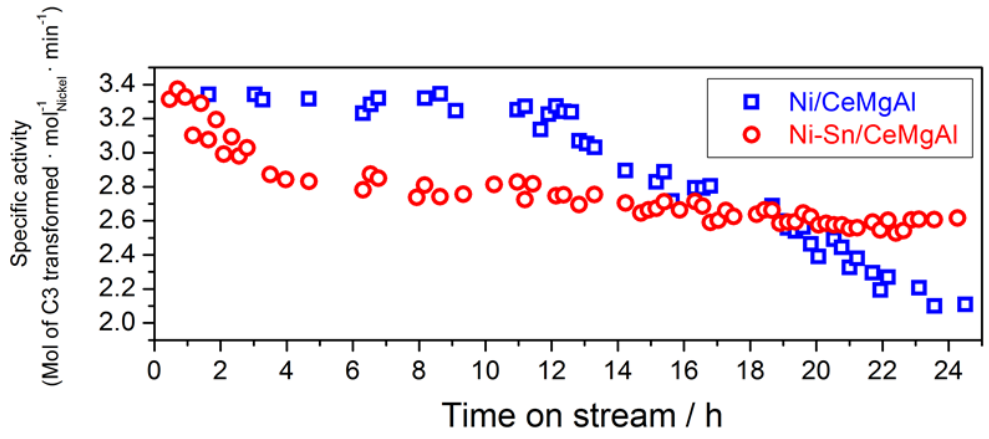

Fig. 4 Catalytic activity as a function of time for glycerol steam reforming at 750ºC for the prepared catalysts

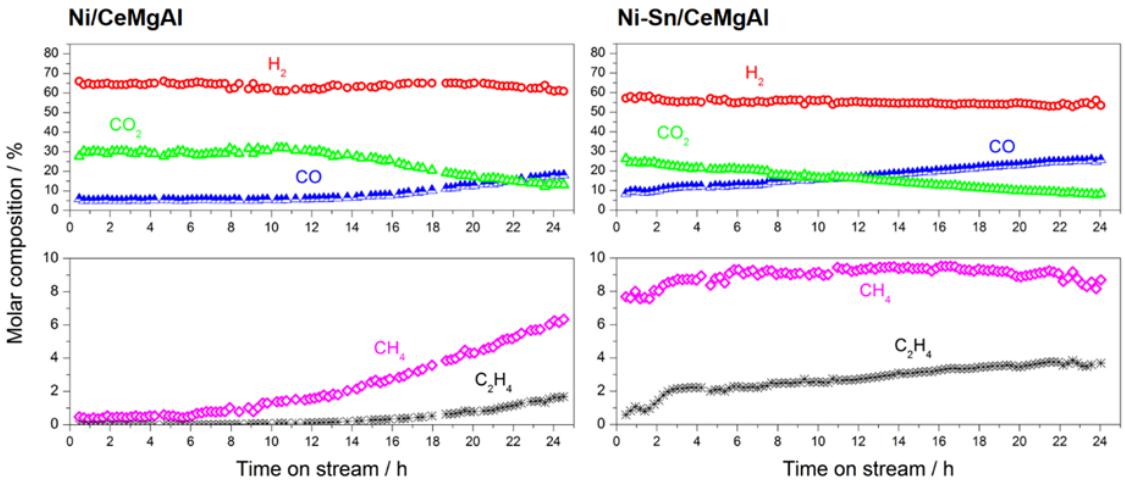

Fig. 5 Product distribution in glycerol steam reforming at 750ºC for the studied catalysts

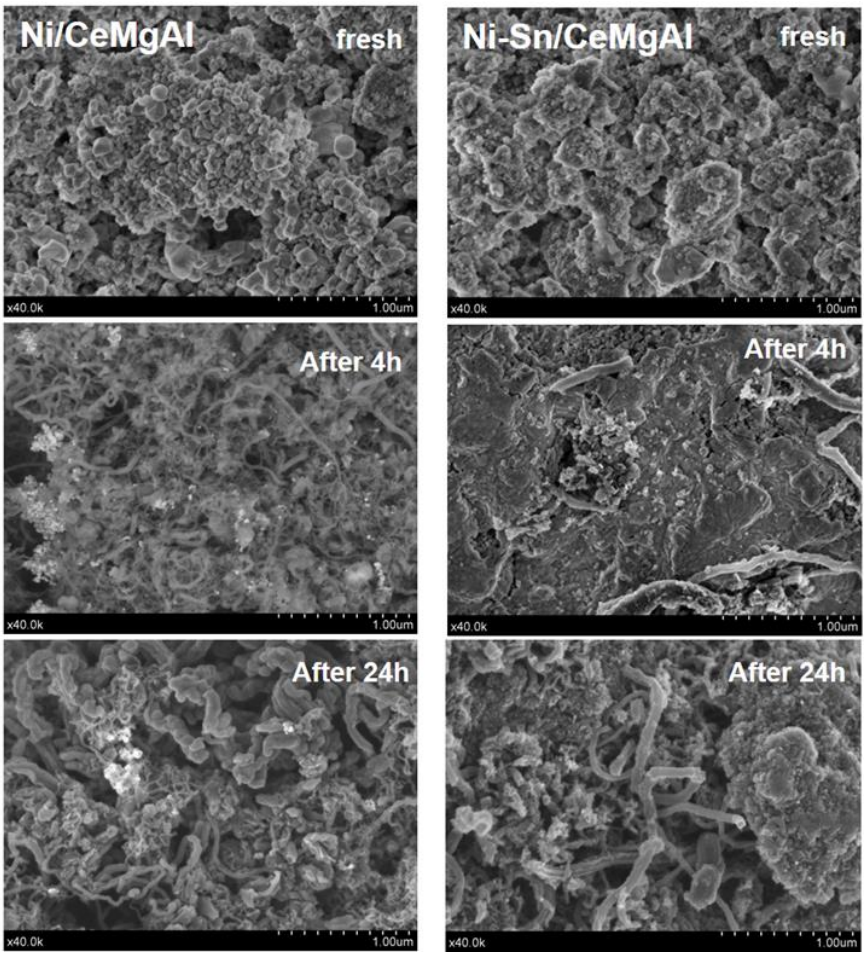

Fig. 6 SEM micrograph of the fresh and used catalysts, after 4 h and 24 h on stream in glycerol steam reforming at 750 ºC

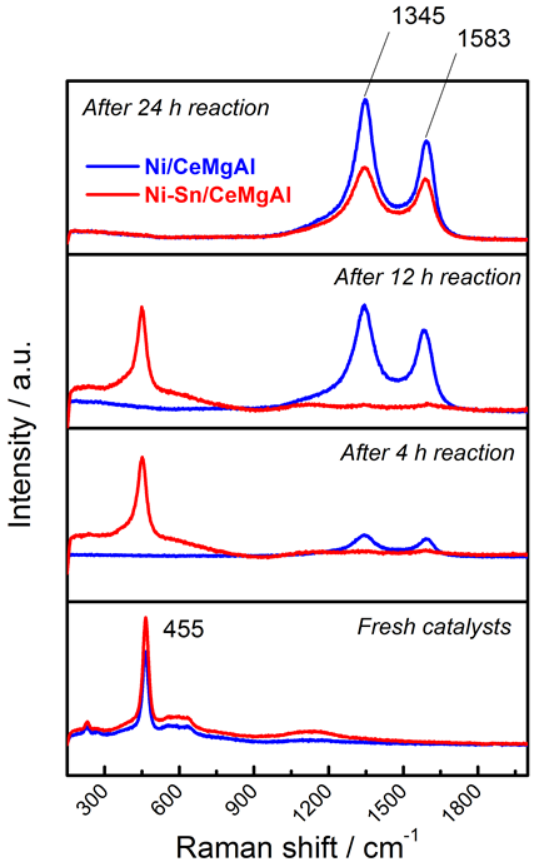

Fig. 7 Raman spectra of fresh and spent catalysts after 4, 12 and 24 h of time on stream at 750 ºC

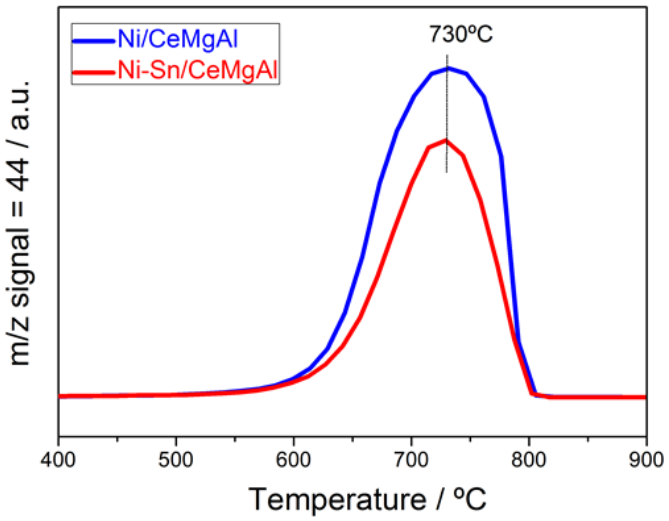

Fig. 8 TPO profiles of both catalysts after 24 h of reaction.

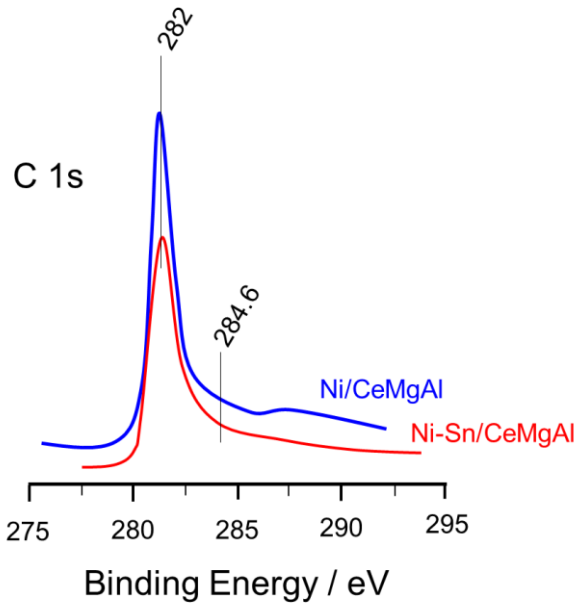

Fig. 9 C 1s region of XPS spectra of both catalysts after 24 h of reaction